Original Research

Frank Spurlock*
Jirka Šimůnek
Bruce Johnson
Atac Tuli

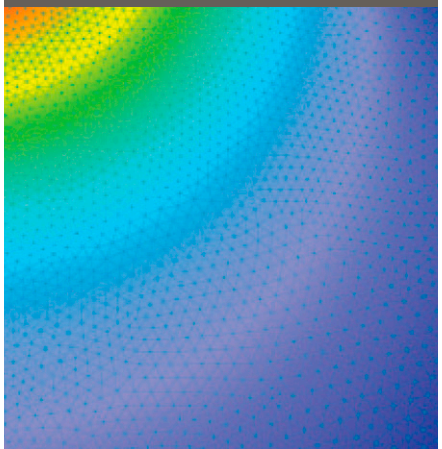

We conducted a comprehensive Monte Carlo sensitivity analysis of fumigant transport and volatilization using HYDRUS. The sensitivities of fumigant flux and soil-gas concentrations varied by application scenario and are interpreted mechanistically. These data provide a reference for designing fumigation field studies and interpreting their results.

F. Spurlock, B. Johnson, and A. Tuli, California Dep. of Pesticide Regulation, 1001 I Street, Sacramento, CA 95812; and J. Šimůnek, Dep. of Environmental Sciences, Univ. of California–Riverside, Riverside, CA 92521. *Corresponding author (fcspurlock@cdpr.ca.gov).

Vadose Zone J.
doi:10.2136/vzj2012.0130
Received 7 Sept. 2012.

Sensitivity Analysis of Soil Fumigant Transport and Volatilization to the Atmosphere

Interest in the use of vadose zone transport models for fumigant risk assessment is increasing. Good modeling practice includes an assessment of model sensitivity and output uncertainty. This computational study evaluated the sensitivity of HYDRUS-1D- and HYDRUS 2D/3D-simulated fumigant cumulative flux, maximum 6-h period mean flux density, and soil gas concentrations to 15 model input variables using Monte Carlo Latin hypercube analysis. The input variables included fumigant physicochemical properties, agricultural film (tarp) properties, and soil properties. Three different application scenarios were investigated: tarped broadcast, tarped bedded shank injection, and a tarped drip line-source application. Model sensitivity to initial water content (θ_i), saturated water content (θ_s), and tarp permeability varied among scenarios depending on the relative importance of soil gas diffusive resistance and tarp mass transfer resistance to fumigant volatilization. Model outputs were sensitive to fumigant air–water partition and gas-phase diffusion coefficients, two parameters that probably have a small contribution to overall modeling uncertainty because accurate estimation methods for these parameters are available. Sensitivities to the fumigant degradation rate were high in all scenarios, and sensitivity to tarp permeability was high only when substantial volatilization occurred from the tarped portion of soil surfaces. Existing literature data for both degradation and tarp permeability are highly variable; parameterizing these processes using literature estimates may contribute substantially to model uncertainty. In several cases, the highest output sensitivities were to θ_s. For model comparisons to site-specific field data, soil texture-based estimates of θ_s are potentially large contributors to model uncertainty; direct measurement is recommended.

Soil fumigants accounted for >20% of the 65 million kg of pesticide active ingredients applied in 2009 California production agriculture. Application rates are on the order of 100 kg ha^{-1} and methods vary, including broadcast subsurface shank injection at 25- to 60-cm depths, bedded shank injection, and chemigation applications through surface and subsurface drip irrigation systems. Agricultural plastic films ("tarps") are usually used to cover the soil surface, either partially or completely, to reduce fumigant volatilization into the atmosphere.

Volatile organic compound emissions, including those from fumigants, are regulated in areas of California that do not meet ozone air quality standards because they are ozone precursors (Marty et al., 2010). Post-application emissions vary by fumigant and application method, and are quantified by the cumulative flux or emission ratio (cumulative flux/fumigant applied). Peak emissions are used to estimate off-site air concentrations, which in turn serve as the basis for buffer zones to limit bystander exposure (Sullivan et al., 2004). Agronomists concerned with efficacy typically evaluate soil gas concentrations and their persistence in the soil profile (Ha et al., 2009).

Field studies to estimate fumigant flux are expensive and generally yield uncertain flux estimates (Majewski, 1997; Ross et al., 1996; Wang et al., 2006; Sullivan et al., 2004). Interest in fumigant transport modeling is increasing, and several models have been used to estimate laboratory- and field-scale fumigant transport and volatilization from soils, including CHAIN-2D (Šimůnek and van Genuchten, 1994), HYDRUS-1D (Šimůnek et al., 2008a), HYDRUS 2D/3D (Šimůnek et al., 2011), and HWC-MODEL (Ha et al., 2009). The governing equations and associated boundary conditions for simultaneous solution of transient water flow and convective–dispersive transport of heat and solute are quite similar among most vadose zone transport models. Critical aspects of simulating fumigant transport in the vadose zone, however, also include the strong temperature dependence of tarp permeabilities (Papiernik et al., 2011), post-application tarp perforation and subsequent removal, and the requirement for two volatilization boundary conditions in situations where only a portion of the field is covered by a tarp. Both HYDRUS-1D (Šimůnek et al., 2008a) and HYDRUS 2D/3D (Šimůnek et al., 2011) simulate tarp dynamics, while HYDRUS 2D/3D also simulates dual surface volatilization boundary conditions and complex field geometries in two or three dimensions. Several recent studies have used the HYDRUS models or their legacy DOS-based precursor CHAIN-2D to describe fumigant transport (Luo et al., 2012; Yates et al., 2012; Luo et al., 2011; Yates, 2009; Cryer and van Wesenbeeck, 2009, 2010).

Sensitivity analysis is a basic component of model evaluation (Crout et al., 2008; Warren-Hicks et al., 2002; van den Berg et al., 2008). Ha et al. (2009) evaluated the sensitivity of 1- and 2-d methyl isothiocyanate soil gas concentrations to temperature-dependent partitioning and degradation parameters in a study of tarped raised beds. The degradation rate was more important than Henry's Law constant or the gas-phase diffusion coefficient in that study. Cryer and van Wesenbeeck (2010) evaluated the sensitivity of cumulative flux to various parameter groups using the legacy model CHAIN-2D for a single application scenario. They concluded that soil water content and tarp properties were among the most important parameters controlling cumulative flux based on rank correlations between inputs and outputs. Neither study provided detailed sensitivities of multiple output variables in multiple application scenarios.

The objectives of this study were to: (i) determine quantitative sensitivities of HYDRUS-1D- and HYDRUS 2D/3D-simulated fumigant cumulative flux, period mean flux densities, and soil gas concentrations to 15 key model inputs in three application scenarios, (ii) interpret those sensitivities from a mechanistic standpoint, and (iii) qualitatively evaluate potential sources of uncertainty in the model output based on the sensitivity analysis. These results will inform sampling strategies for designed studies to compare field-based and model-simulated flux estimates and facilitate interpretation of simulation results.

Methods

Overview

Two analyses were conducted in this computational study. A preliminary analysis evaluated the sensitivity of the fumigant effective gas-phase diffusion coefficient in soil (D_{eff}, Eq. [6] below) and the effective soil–air surface boundary layer mass transfer coefficient (K_{MTC}, Eq. [8] below) to seven variables (Table 1) using a Monte Carlo Latin hypercube sensitivity analysis method. This preliminary analysis aided interpretation of the relative importance of diffusive resistance vs. surface mass transfer resistance to post-application fumigant volatilization in the second full sensitivity analysis.

The second analysis used the Latin hypercube method to evaluate the relative sensitivity of 50-d cumulative flux, maximum 6-h average flux density (μg cm^2 d^{-1}), and maximum shallow soil gas concentration (μg cm^{-3}) to 15 input variables. The input variables included fumigant physicochemical properties, properties of the tarp, soil properties, and amplitude of soil surface diurnal temperature fluctuations (Table 1). Each application was simulated to occur at 0600 h. Maximum 6-h mean flux densities were determined for post-application periods of 0600 to 1200 h, 1200 to 1800 h, 1800 to 2400 h, etc., such as would be reported for a typical field flux experiment. Three fumigant application scenarios were considered: a fully tarped broadcast application simulated with a one-dimensional modeling domain (broadcast scenario, Fig. 1a), a tarped bedded shank application with untarped furrows simulated with a two-dimensional modeling domain (bed scenario, Fig. 1b), and an under-tarp bedded drip application simulated using a line source representation in a two-dimensional modeling domain (drip scenario) (Fig. 2).

Table 1. Input variables used in the sensitivity analyses.

Variable†	Description	Median	Range (min.–max.)
d, cm†	boundary layer thickness	425	50–800
dE_a, J mol^{-1} K^{-1}	boundary layer activation energy	−40,000	−60,000 to −20,000
ΔT, °C	daily temperature amplitude	12.5	5–20
D_g, cm^2 d^{-1}†	gas-phase diffusion coefficient	8,250	6,500–10,000
D_gE_a, J mol^{-1} K^{-1}	D_g activation energy	4,650	4,500–4,800
λ_w, cm	longitudinal dispersivity	10.5	1–20
D_w, cm^2 d^{-1}	aqueous-phase diffusion coefficient	0.85	0.7–1.0
k_1, d^{-1}	degradation rate constant	0.36	0.03–0.69
k_1E_a, J mol^{-1} K^{-1}	k_1 activation energy	52,500	40,000–65,000
K_h†	air–water partition coefficient	0.15	0.05–0.25
K_hE_a, J mol^{-1} K^{-1}	K_h activation energy	30,000	20,000–40,000
K_d, mL g^{-1}†	soil–water partition coefficient	0.206	0.0375–0.375
ρ_b, g cm^{-3}†	soil bulk density	1.54	1.28–1.80
θ_i, cm^3 cm^{-3}†	initial soil water content	0.13	0.06–0.20
θ_s, cm^3 cm^{-3}†	saturated soil water content	0.42	0.30–0.54

† Included in both preliminary sensitivity analyses of effective diffusion coefficient D_{eff} and surface mass transfer coefficient K_{MTC} and main sensitivity analysis. All others used in main sensitivity analysis only.

Simulation of Water, Solute, and Heat Transport

Both HYDRUS programs simultaneously solve the Richards equation for variably saturated water flow and the advection–dispersion equations for heat and solute transport. Solutions to those flow and transport equations are solved numerically subject to specified

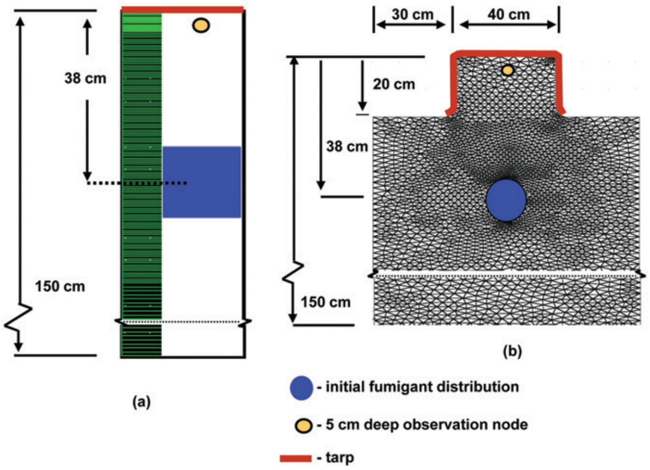

Fig. 1. (a) One-dimensional tarped broadcast and (b) two-dimensional tarped bedded shank application modeling domains. The one-dimensional figure shows nodal density on the left, initial fumigant distribution on the right. Width (a) and diameter (b) of initial fumigant distribution was ∼15 cm.

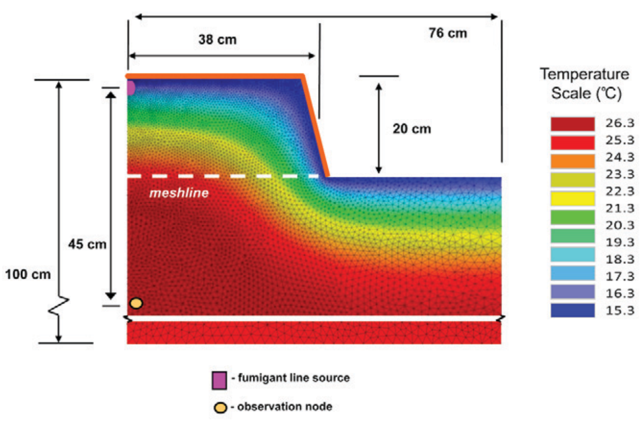

Fig. 2. Two-dimensional tarped bed drip domain (line source representation). Initial soil profile temperature conditions at 0600 h on day of application shown. Defined mesh line used to evaluate water fluxes out of the bed.

boundary conditions using Galerkin-type linear finite elements in one (HYDRUS-1D), two, or three dimensions (HYDRUS 2D/3D) depending on the problem (Šimůnek et al., 2008b). The heat transport equation considers conduction and convection with flowing water, while the solute transport equations consider advective and diffusive–dispersive transport in the liquid phase and diffusion in the gas phase.

For all simulations, the relationship between soil water content (θ) and pressure head (h) was

$$\theta(h) = \theta_r + \frac{\theta_s - \theta_r}{\left(1+|\alpha h|^n\right)^{1-1/n}}; h<0 \qquad [1]$$
$$= \theta_s \qquad ; h \geq 0$$

where θ_r is the residual water content (cm^3 water cm^{-3} bulk soil), θ_s is the saturated water content, and α (cm^{-1}) and n are empirical constants (van Genuchten, 1980).

The Water Linear Reduction gas-phase tortuosity model (Moldrup et al., 2000) was used to describe gas-phase tortuosity, τ_g, in all simulations:

$$\tau_g = \frac{a_v^{1.5}}{\theta_s} \qquad [2]$$

where θ_s in this case represents total porosity and a_v is the air-filled porosity (cm^3 air cm^{-3} bulk soil). Tortuosity reduces the effective gas-phase diffusion of a fumigant in soil relative to that in air. Fumigant gas-phase diffusive flux density in the soil is proportional to the spatial concentration gradient:

$$J = -a_v \tau_g D_g \frac{\partial C_g}{\partial x} \qquad [3]$$

where J is flux density (µg cm^{-2} d^{-1}) in the x direction, D_g is the fumigant diffusion coefficient in air (cm^2 d^{-1}), and C_g is the fumigant gas-phase concentration (µg cm^{-3} air), which is related to the total soil fumigant concentration C_T (aqueous + sorbed + gas, µg cm^{-3} soil) through an equilibrium partition coefficient R_g:

$$C_g = \frac{C_T}{R_g} \qquad [4]$$

$$R_g = \frac{\rho_b K_d}{K_h} + \frac{\theta}{K_h} + a_v \qquad [5]$$

where K_d (mL g^{-1}) is the linear equilibrium soil water distribution coefficient, ρ_b is soil bulk density (g cm^{-3}), and K_h is the dimensionless air–water partition coefficient. When the spatial gradient in C_T is used in Eq. [3], the corresponding effective fumigant gas-phase diffusion coefficient D_{eff} in bulk soil is obtained by combining Eq. [2–5]:

$$D_{eff} = \frac{K_h D_g (\theta_s - \theta)^{2.5}}{\theta_s \left[\rho_b K_d + \theta + (\theta_s - \theta) K_h\right]} \qquad [6]$$

where θ is soil water content and a_v is assumed equal to $\theta_s - \theta$. The effective diffusion coefficient D_{eff} is applicable to total fumigant concentration and accounts for tortuosity of the air-filled soil pore space, the reduction in cross-sectional area due to the presence of the soil solid phase, and fumigant partitioning among the solid, aqueous, and gas phases.

Boundary Conditions

Atmospheric water flow boundary conditions (BCs) were applied at the top surface of all modeling domains. The potential flux in that BC is controlled by external specified time-variable precipitation and potential evaporation fluxes (Šimůnek et al., 2011). No precipitation was simulated in any of the scenarios. The potential evaporative flux was set to zero for the tarped portion of each modeling domain, while daily potential evaporation of 6.8 mm was used for the untarped portion of the soil surfaces. This potential evaporation corresponds to early summer reference evapotranspiration rates in California's San Joaquin Valley and was simulated between 0700 and 1700 h daily, with the maximum rate between 1000 and 1600 h. For atmospheric BCs, actual evaporation is also determined by a limiting critical pressure head at the soil surface. Below that critical pressure head, actual evaporation is less than potential evaporation. That critical pressure head was defined as the HYDRUS default of −15,000 cm based on preliminary simulations that showed minimal effect of that parameter. At the lower boundary, a unit hydraulic gradient (free drainage) BC was applied in all scenarios.

A stagnant layer volatile solute BC was applied at the top of all modeling domains. That BC describes fumigant surface volatilization flux density J (μg cm^{-2} d^{-1}) through a boundary of thickness d (cm) as

$$\begin{aligned} J &= \frac{D_g}{d}\left[C_g(0) - C_g(d)\right] \\ &= k_{\mathrm{MTC}}\left[C_g(0) - C_g(d)\right] \end{aligned} \qquad [7]$$

where $C_g(0)$ and $C_g(d)$ are the solute gas-phase concentrations at the soil surface and at the top of the equivalent boundary layer of thickness d, respectively, and k_{MTC} (cm d^{-1}) is a first-order mass transfer coefficient (Jury et al., 1983). The value of $C_g(d)$ was assumed equal to zero in all cases. The equivalent boundary layer thickness d has no physical meaning but represents a mass transfer resistance at the soil surface. Appropriate d values may be estimated for any fumigant–tarp combination from standard tarp k_{MTC} measurements (Papiernik et al., 2011). For untarped bare soil areas, d = 0.5 cm was assumed (Jury et al., 1983), while d values ranging up to 800 cm were used to simulate mass transfer resistance in tarped regions based on polyethylene tarp fumigant permeability data (Papiernik et al., 2011). At the bottom of each modeling domain, the solute BC was a Cauchy (third-type) BC, where fumigant flux out of the domain is the product of the fumigant aqueous concentration and water flux.

Combining Eq. [5] and [7] gives the effective mass transfer coefficient K_{MTC} applicable to the total fumigant concentration C_{T} (Jury et al., 1983):

$$\begin{aligned} K_{\mathrm{MTC}} &= \frac{k_{\mathrm{MTC}}}{R_g} \\ &= \frac{K_h D_g}{d\left[\rho_b K_d + \theta + (\theta_s - \theta) K_h\right]} \end{aligned} \qquad [8]$$

Soil surface temperature was assumed to vary sinusodially with time:

$$T(t) = T_0 + \Delta T \sin\left[\pi\left(2t - \frac{7}{12}\right)\right] \qquad [9]$$

where t is time (d), T_0 is the average temperature, assumed here to be 25°C, and ΔT is the amplitude of the daily fluctuation. Default volumetric heat capacities for soil constituents and default thermal conductivity parameters for sands (Chung and Horton, 1987) were used. The volume fraction of soil mineral components for each simulation was specified as $(1 - \theta_s)$.

The temperature dependence of the diffusion coefficients, air–water distribution constant, degradation rate constant, and boundary layer depth d were simulated using an Arrhenius-type relationship (Šimůnek et al., 2011):

$$x_{i,T} = x_{i,\mathrm{r}} \exp\left[\frac{E_a}{R}\left(\frac{1}{T_\mathrm{r}} - \frac{1}{T}\right)\right] \qquad [10]$$

where $x_{i,T}$ is the value of the desired coefficient at temperature T (K), $x_{i,\mathrm{r}}$ is the value at the reference temperature T_r = 293 K, R is the universal gas constant = 8.314 J mol^{-1} K^{-1}, and E_a (the "activation energy," J mol^{-1}) is the proportionality constant between $\ln(x_i)$ and the reciprocal temperature. While the various E_a values in Table 1 are not true activation energies in a chemical thermodynamic sense, the "activation energy" terminology is retained here to maintain consistency with the historical Arrhenius relationship.

Fumigant Application Scenarios and Initial Conditions

The geometric configuration of the one-dimensional broadcast, two-dimensional bed, and two-dimensional drip applications, discretization, and initial fumigant concentration conditions are shown in Fig. 1 and 2. Soil profiles were uniform, and the vertical modeling domain depths were arbitrarily chosen as 100 cm based on preliminary simulations that demonstrated little effect of depth on fumigant volatilization flux beyond that value. The initial profile soil temperature in each scenario was taken as the final temperature distribution obtained in 5.25-d preliminary simulations using an average soil temperature of 25°C and an amplitude of 12.5°C (Eq. [9]). In all scenarios, 100 kg ha^{-1} applications were simulated at 0600 h on Day 1. All simulations were conducted for an arbitrary "long" period of 50 d to ensure complete fumigant volatilization or degradation. Observation nodes were defined in each modeling domain to obtain simulated soil gas concentrations at the end of each 6-h interval (Fig. 1 and 2). The observation nodes were situated approximately 50 cm away from the region where the fumigant was applied (Fig. 1 and 2). For the bed and broadcast applications, these nodes were near the tarp surface; in the drip scenario, the nodes were below the drip line source. The end-of-simulation fumigant mass balance errors for 1200 simulations in each scenario, expressed as percentage of the initial application, were 0.2, 0.4, and 0.7% (broadcast), 0.7, 1.0, and 1.5% (bed), and 0.7, 1.0, and 1.5% (drip) for the 10th, 50th, and 90th percentile, respectively.

A majority of California fumigant applications occur in sandy loam soils (Johnson and Spurlock, 2009), and average values for the sandy loam texture for residual water content θ_r (0.039), α (0.029 cm^{-1}), n (1.45) (Schaap et al., 2001), and saturated hydraulic conductivity K_s (106 cm d^{-1}) (Carsel and Parrish, 1988) were used in all simulations. Saturated water content θ_s was varied to determine the model output sensitivity to that variable (Table 1).

In the drip scenario, the fumigant chemigation was simulated with a water application of 288 cm^2 during 13.2 h, corresponding to a drip-line water application rate of 4.4 L m^{-1} h^{-1}. The application was simulated through a 2.5-cm-diameter line source 1 cm below the soil surface (Fig. 2). The fumigant concentration was 373 μg L^{-1} and the water temperature was 12°C.

Latin Hypercube Sensitivity Analysis

Latin hypercube sampling is efficient in obtaining representative samples across the entire input parameter space (McKay et al., 1979). The Latin hypercube sensitivity analysis method used in this study was similar to that reported by van Griensven et al. (2006), originally adapted from the basic method of Morris (1991). For a model output M that is a function of N input parameters (x_1, ..., x_N), a sensitivity index S_i is defined that describes the effect of a perturbation Δx_i of model input x_i, with the remaining parameters x_{ji} constant:

$$S_i = \frac{M(x_1,...x_i+\Delta x_i,...x_N) - M(x_1,...x_i,...x_N)}{\left[M(x_1,...x_i+\Delta x_i,...x_N) + M(x_1,...x_i,...x_N)\right]/2} \times \frac{x_i}{\Delta x_i} \qquad [11]$$

The individual S_i are point estimates of the normalized partial derivative of M with respect to x_i, so are local measures of sensitivity. Latin hypercube sampling was used to estimate the mean S_i (denoted here as μ_i) across the entire N-dimensional parameter hyperspace. The standard deviation of S_i (= σ_i) across that same parameter space provides a measure of the interaction between x_i and the other inputs and of the nonlinear effect of x_i on the dependent variable M (Morris, 1991; Saltelli et al., 2005).

The procedure for estimating μ_i and σ_i was to (i) randomly select a single value from each decile of each of the N assumed uniform x_i distributions, (ii) form 10 vectors of input parameters (x_1, ..., x_N) by randomly selecting one x_i without replacement from each sample drawn in the first step, (iii) run the model using each of those 10 (x_1, ..., x_N) input vectors, and (iv) again run the model using each of the 10 input vectors but with the perturbed value $x_i + \Delta x_i$ substituted for x_i. Thus, for each x_i, 20 model runs were conducted, yielding 10 estimates of S_i. The perturbations Δx_i were taken as $\pm$10% of the base x_i, with the sign of the perturbation randomly selected.

For both the preliminary and full sensitivity analyses, a single trial consisted of estimating 10 S_i for each of the input variables (Table 1). Results from four trials were then used to calculate the mean sensitivities μ_i and standard deviation σ_i for each input variable–dependent output variable combination. In the preliminary sensitivity analysis, D_{eff} (Eq. [6], six input variables) and K_{MTC} (Eq. [8], seven input variables) were the dependent variables (M, Eq. [11]), and that analysis was conducted using a spreadsheet.

In the second main sensitivity analysis, there were 15 input variables × 20 simulations per variable = 300 HYDRUS simulations per trial for each modeling scenario (broadcast, bed, and drip). The dependent variables were cumulative flux, maximum 6-h flux density, and soil gas concentration.

Input Variables Evaluated in Sensitivity Analyses

The preliminary analysis estimated sensitivities S_i of D_{eff} (Eq. [6]) and K_{MTC} (Eq. [8]) with respect to D_g, K_h, ρ_b, K_d, d, θ, and θ_s (Table 1), while the second analysis evaluated the sensitivity of HYDRUS outputs to all 15 variables listed in Table 1. Each chemical property input was assigned a uniform distribution based on the approximate ranges of published or estimated data for 1,3-dichloropropene, chloropicrin (trichloronitromethane), methyl bromide, and methyl iodide (Table 1). Ranges for aqueous and gas-phase fumigant diffusion coefficients (Table 1) were based on estimates from the on-line SPARC calculator (http://archemcalc.com/sparc.php, Hilal et al., 2003a, 2003b), while the gas-phase diffusion activation energy was calculated from SPARC D_g estimates as a function of temperature. The range of dimensionless Henry's Law constants were obtained from the literature (Kim et al., 2003; Glew and Moelwyn-Hughes, 1953; Ruzo, 2006). Henry's Law activation energies were measured or estimated from enthalpy of vaporization data (USEPA. 2001; Kim et al., 2003; Chickos and Acree, 2003; Glew and Moelwyn-Hughes, 1953). The range of fumigant soil degradation rates were based on the compilation of Dungan and Yates (2003), and the range of degradation activation energies were based on the variation in aerobic degradation rates with temperature reported by Dungan and Yates (2003), Gan et al. (2000), and Guo and Gao (2009). The range for soil water partition coefficients was calculated using organic C normalized soil partition K_{OC} data from the California Department of Pesticide Regulation pesticide chemistry database of registrant data submissions and the EU FOOTPRINT database (http://sitem.herts.ac.uk/aeru/

footprint/en/), assuming a soil mass fraction organic C of 0.005. While enhanced vapor sorption coefficients have been reported for very dry soil conditions, we assumed this mechanism to be of minor importance in our scenarios due to (i) fumigant label preapplication requirements that specify soil water contents at the 20-cm depth of at least 50% of the available water content, (ii) the presence of a tarp fully or partially covering the soil surface, which minimizes evaporation, (iii) low clay contents of sandy loam soils (<20%), and (iv) the small and nonpolar nature of fumigant molecules, especially methyl bromide, 1,3-dichloropropene, and methyl iodide. These factors reduce sorption enhancement effects (Petersen et al., 1996).

The uniform initial soil water content θ_i spanned the approximate range of 50 to 75% of sandy loam water contents at field capacity (h = −300 cm) as calculated from data in the UNSODA database (Leij et al., 1996). The range of saturated water contents and bulk densities were chosen from UNSODA data for sandy loam soils. In the preliminary analysis, the uniform distribution of θ_i (Table 1) was used as the sampling distribution for θ in Eq. [6] and [8]. The dispersivity maximum and minimum were based on approximate ranges for soil columns and field soils (Radcliffe and Šimůnek, 2010, p. 249–346). The boundary layer depth and activation energy d and dE_a were calculated from the polyethylene tarp permeability data of Papiernik et al. (2011). The upper bound for the daily temperature amplitude of 20°C was based on reported under-tarp field temperature data (Yates et al., 2002).

Results

Initial Sensitivity Analysis of the Gas-Phase Diffusion and Boundary Layer Mass Transfer Coefficients

The sensitivity analysis of D_{eff} (Eq. [6]) and K_{MTC} (Eq. [8]) assumed isothermal conditions, so the resulting μ_i are only a general guide to the relative importance of input variables to the simulated processes. As expected from Eq. [6] and [8], the respective sensitivities of D_{eff} and K_{MTC} to K_h, D_g, K_d, and ρ_b were identical (Table 2). Sensitivities to ρ_b and K_d were essentially identical because these variables only occur together as a product in both Eq. [6] and Eq. [8]. The principal differences between D_{eff} and K_{MTC} were their sensitivities to θ and θ_s, and to d, which only appears in Eq. [8]. Both θ and θ_s influence fumigant partitioning through the denominator of both equations, but partitioning effects on D_{eff} are overshadowed by their role in determining tortuosity. Hence, diffusive transport is particularly sensitive to both θ and θ_s (Table 2).

General Comparison of the Modeling Scenarios

Across all 1200 simulations for each scenario, median 50-d emission ratios for the broadcast, bed, and drip application scenarios were 0.10 (0.02 and 0.33 for the 10th and 90th percentiles, respectively), 0.21 (0.05 and 0.50) and 0.32 (0.17 and 0.61), respectively (Fig. 3a). In the bed scenario, the majority of fumigant volatilization occurred from the untarped portion of the soil surface; the median fraction of total cumulative volatilization from the untarped soil area was 0.90 (0.83 and 0.94 for the 10th and 90th percentiles, respectively). In contrast, the fraction of total volatilization from untarped soil in the drip scenario was only 0.11 (0.02 and 0.28 for the 10th and 90th percentiles, respectively). Maximum 6-h mean flux densities displayed the same trend among scenarios as the emission ratios, with medians of 56 μg cm^{-2} d^{-1} for the broadcast scenario, 132 μg cm^{-2} d^{-1} in the bed scenario, and 286 μg cm^{-2} d^{-1} in the drip scenario (Fig. 3b). Maximum soil gas concentrations were similar among scenarios, with median concentrations of 1 to 2 μg cm^{-3} (Fig. 3c).

Table 2. Mean (μ_i) and standard deviation (σ_i) of effective gas-phase diffusion coefficient (D_{eff}, Eq. [6]) and boundary layer mass-transfer coefficient (K_{MTC}, Eq.[8]) sensitivities to independent variables in the preliminary analysis.

Variable†	D_{eff}		K_{MTC}	
	μ_i	σ_i	μ_i	σ_i
d	–	–	−0.99	0.05
ρ_b	−0.62	0.17	−0.62	0.17
K_d	−0.62	0.15	−0.62	0.15
θ_i	−1.44	0.59	−0.24	0.10
θ_s	2.62	0.79	−0.14	0.07
K_h	0.90	0.09	0.90	0.09
D_g	0.99	0.05	0.99	0.05

† d, boundary layer thickness; ρ_b, soil bulk density; K_d, soil–water partition coefficient; θ_i, initial soil water content; θ_s, saturated soil water content; K_h, air–water partition coefficient; D_g, gas-phase diffusion coefficient.

General differences in temporal flux dynamics and gas concentrations at the observation points among the three application scenarios are illustrated in Fig. 4. These simulations used the median of each input variable (Table 1). For each scenario, the temporal flux patterns across all 1200 simulations were generally similar to those shown in Fig. 4a. In the drip scenario, the maximum 6-h mean flux density always occurred in the afternoon (1200–1800 h) or evening (1800–2400 h) of the day of application, and those fluxes were generally quite high compared with the bed and broadcast scenarios. In the bed scenario, 25% of maximum period mean flux densities occurred during the second (1200–1800 h) period on the day of application, but the majority (60%) were during 0600 to 1200 or 1200 to 1800 h during Day 2. The timing of the maximum period mean flux density in the broadcast scenario was similar to the bed scenario, but the magnitude of those peak fluxes was generally lower (e.g., Fig. 4a).

Gas concentrations at the observation points were "instantaneous" concentrations at the end of each 6-h period. While the drip scenario observation node was located 45 cm below the drip line, these concentrations were generally comparable in magnitude to

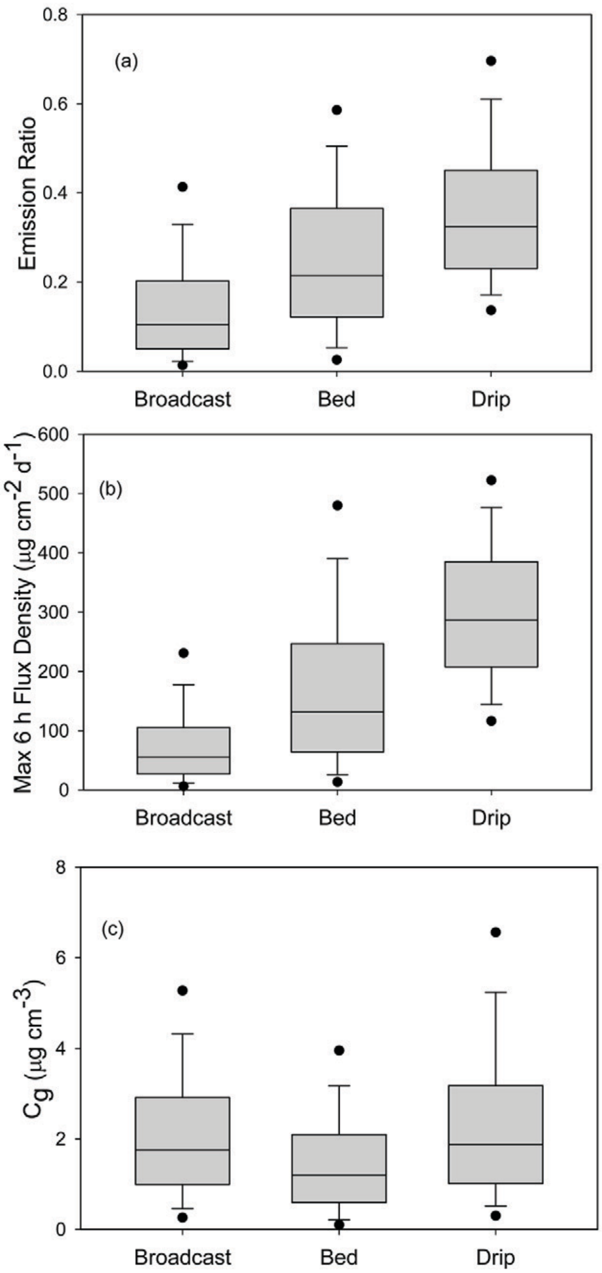

Fig. 3. Box plots of (a) emission ratio, (b) maximum 6-h flux density, and (c) maximum fumigant soil gas concentration C_g for broadcast, bed, and drip application scenarios, showing median (center line), quartiles (box boundaries), 10th and 90th percentile (whiskers), and 5th and 95th percentiles (symbols) based on N = 1200 simulations for each scenario.

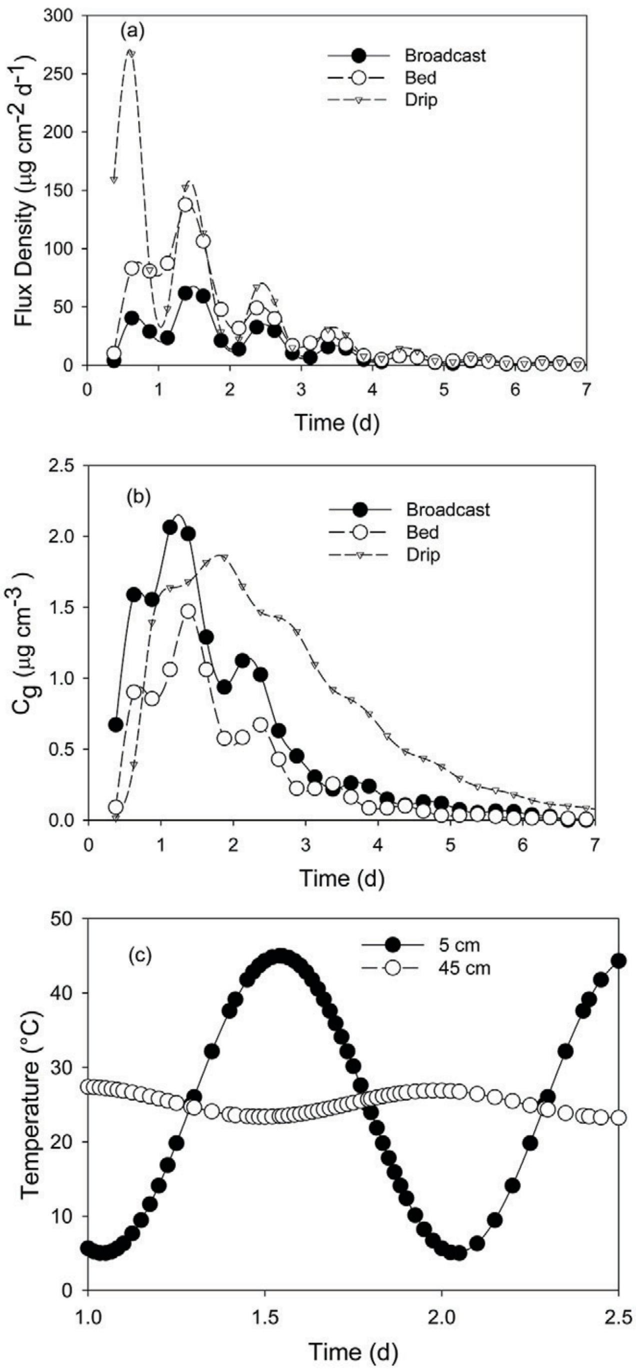

Fig. 4. Illustrative comparison of (a) simulated maximum 6-h mean flux densities, (b) maximum post-application soil gas concentrations C_g, and (c) soil temperature fluctuations at the 5- and 45-cm depths. Median values of input variables were used in all simulations (Table 1).

the shallow concentrations simulated in the other two scenarios (Fig. 4b). There was a strong diurnal signal in the shallow gas concentrations but much less so in the drip scenario. This was attributable to the lower temperature fluctuations at the deeper depth (Fig. 4c). The simulated concentrations were comparable to shallow gas concentrations measured in field studies when normalized by the application rate (Gao et al., 2008; Gao and Trout, 2007).

Water flow out of the bottom of the profile was generally very low in the broadcast and bed scenarios. In simulations using median input variables, the cumulative water flux at 50 d was 0.035 and 0.038 cm, respectively, the latter being the average flux across the bottom of the bed domain boundary. Deep drainage was higher in the drip scenario, with a cumulative drainage flux of 0.15 cm (average across the bottom domain boundary), and this corresponded to

~4% of the applied water. The maximum drainage in all scenarios occurred at the highest θ_i (0.20, Table 1). Simulations using θ_i = 0.20 along with the other median input variables yielded mean cumulative water fluxes of 1.3, 1.1, and 2.0 cm for the broadcast, bed, and drip scenarios, respectively. This corresponds to 53% of applied water in the drip scenario.

Sensitivity of Cumulative Flux

While cumulative flux was relatively sensitive to the gas-phase diffusion coefficient D_g and air–water distribution coefficient K_h as expected, the greatest sensitivity was to θ_s for two of the three application scenarios (Table 3). The $\mu_{\theta s}$ for the broadcast and bed cumulative flux (1.6 and 2.1, respectively) gives a mean change in cumulative flux of 16 and 21%, respectively, for a 10% change in θ_s, all other factors being equal (Table 3). In contrast, 10% perturbations to either D_g or K_h yielded nearly equivalent percentage changes in cumulative flux for the broadcast and bed scenarios as seen from their respective μ_i values (Table 3). The high sensitivity of cumulative flux to θ_s in the broadcast and bed scenarios reflects the importance of diffusive transport in those scenarios. The importance of diffusion is also indicated by the large negative sensitivity of cumulative flux to θ_i, consistent with preliminary sensitivity results for D_{eff} and K_{MTC} (Table 2).

Sensitivities for the drip scenario were generally much lower than for the other two scenarios. This was partially attributable to the near-surface application of the drip-applied fumigant directly under the tarp and the corresponding rapid volatilization from the tarped area. The mean fraction of eventual total volatilization that occurred within the first 24 h was 0.54 for the drip application, compared with 0.24 and 0.31 for the broadcast and bed scenarios, respectively. Thus, for the drip scenario, short mean diffusion path lengths and rapid volatilization yielded lower flux sensitivities to diffusion-related variables: D_g, K_h, θ_s, ρ_b, and K_d (Table 3). Initial water content in the drip scenario had only a minor effect on cumulative flux because the post-application water content was dominated by the drip input, similar to the conclusion of Ha et al. (2009). Cumulative flux was sensitive to the degradation rate constant k_1 in all scenarios; however, the shorter fumigant soil residence time in the drip scenario noted above contributed to lower μ_{k1} relative to bed and broadcast applications.

The sensitivity to mass transfer resistance as represented by d (Table 3) varied by application method and was related to the fraction of eventual cumulative volatilization that occurred in the tarped area of the profile. In the bedded shank scenario, only a small portion of the volatilization occurred through the tarp. In that scenario, cumulative flux was essentially insensitive to d (Table 3). In contrast, cumulative flux was much more sensitive to d in the drip and broadcast scenarios, where larger fractions of the total cumulative volatilization occurred through tarped surfaces.

Table 3. Mean (μ_i) and standard deviation (σ_i) of cumulative flux, maximum 6-h mean flux density, and fumigant soil gas concentration sensitivities to 15 input variables for three application scenarios.

Input variable†	Broadcast		Bed		Drip	
	μ_i	σ_i	μ_i	σ_i	μ_i	σ_i
Cumulative flux						
θ_s	1.63	1.45	2.14	1.30	0.44	0.15
D_g	1.03	0.36	0.86	0.35	0.48	0.16
K_h	0.96	0.39	0.81	0.36	0.47	0.17
dE_a	0.21	0.13	0.02	0.01	0.16	0.09
D_gE_a	0.05	0.02	0.01	0.02	0.03	0.01
K_hE_a	0.20	0.12	0.25	0.12	0.18	0.07
ΔT	0.01	0.08	0.00	0.02	0.12	0.12
λ_w	0.00	0.00	0.00	0.00	−0.06	0.04
D_w	0.00	0.00	0.00	0.00	0.00	0.00
k_1E_a	−0.46	0.25	−0.41	0.25	−0.27	0.10
d	−0.47	0.20	−0.04	0.01	−0.28	0.15
ρ_b	−0.63	0.26	−0.54	0.24	−0.17	0.07
K_d	−0.68	0.41	−0.58	0.38	−0.18	0.09
k_1	−1.06	0.49	−0.90	0.51	−0.52	0.13
θ_i	−1.23	1.18	−1.22	1.05	−0.19	0.09
Maximum 6-h mean flux density						
θ_s	2.16	1.68	2.91	1.39	0.16	0.17
D_g	1.31	0.38	1.28	0.44	0.53	0.19
K_h	1.15	0.40	1.19	0.41	0.52	0.20
dE_a	0.43	0.17	0.03	0.06	0.32	0.14
D_gE_a	0.09	0.03	0.05	0.03	0.05	0.02
K_hE_a	0.28	0.17	0.49	0.18	0.29	0.09
ΔT	0.28	0.12	0.23	0.11	0.37	0.18
λ_w	0.00	0.00	0.00	0.01	−0.10	0.05
D_w	0.00	0.00	0.00	0.00	0.00	0.00
k_1E_a	−0.26	0.22	−0.25	0.22	−0.09	0.07
d	−0.54	0.19	−0.06	0.02	−0.45	0.19
ρ_b	−0.83	0.33	−0.80	0.31	−0.19	0.07
K_d	−0.92	0.46	−0.85	0.39	−0.20	0.08
k_1	−0.56	0.45	−0.49	0.46	−0.09	0.05
θ_i	−1.57	1.19	−1.77	1.20	−0.13	0.08
Maximum fumigant soil gas concentration						
θ_s	1.45	1.24	1.95	1.73	−0.83	1.02
D_g	0.31	0.32	0.51	0.67	0.14	0.24
K_h	1.17	0.35	1.39	0.60	1.06	0.26
dE_a	−0.07	0.06	−0.11	0.07	−0.02	0.01
D_gE_a	0.01	0.02	−0.02	0.03	0.00	0.01
K_hE_a	0.35	0.17	0.55	0.21	0.25	0.06
ΔT	0.03	0.09	0.08	0.10	−0.05	0.07
λ_w	0.00	0.00	0.00	0.00	0.55	0.33
D_w	0.00	0.00	0.00	0.00	0.00	0.00
k_1E_a	−0.23	0.17	−0.36	0.31	−0.38	0.29
d	0.20	0.08	0.20	0.07	0.02	0.02
ρ_b	−0.81	0.30	−0.92	0.36	−1.08	0.45
K_d	−0.84	0.41	−0.98	0.53	−1.10	0.61
k_1	−0.55	0.40	−0.70	0.63	−0.64	0.31
θ_i	−1.18	1.01	−1.60	1.47	0.14	0.34

† θ_s, saturated soil water content; D_g, gas-phase diffusion coefficient; K_h, air–water partition coefficient; dE_a, boundary layer activation energy; D_gE_a, D_g activation energy; K_hE_a, K_h activation energy; ΔT, daily temperature amplitude; λ_w, longitudinal dispersivity; D_w, aqueous-phase diffusion coefficient; k_1E_a, degradation rate constant activation energy; d, boundary layer thickness; ρ_b, soil bulk density; K_d, soil–water partition coefficient; k_1, degradation rate constant; θ_i, initial soil water content.

Cumulative flux was relatively insensitive to parameters that control temperature-dependent partitioning and transport (Table 3). This supports previous suggestions that simple isothermal models may be adequate for screening purposes if diurnal flux dynamics are unimportant (Yates et al., 2002). In all scenarios, cumulative flux was insensitive to D_w and λ_w, variables that describe transport in the aqueous phase.

Sensitivity of Maximum Six-Hour Mean Flux Density

While the sensitivities of 6-h mean flux densities were generally similar to those of cumulative flux in many cases, there were some differences. First, sensitivities to K_d and ρ_b in the broadcast and bed applications were somewhat greater. The sensitivities of these two variables were essentially equal because their only computational role in HYDRUS is in phase-partitioning calculations (e.g., Eq. [5]). In this role, they only occur together as a product, hence a fixed percentage perturbation to either K_d or ρ_b has an equivalent effect on all model outputs.

Another difference between cumulative flux and maximum 6-h period mean flux densities was for the variables that control the temperature dependence of air–water partitioning and surface mass transfer resistance, K_hE_a, dE_a, and ΔT. Higher K_hE_a or ΔT yielded higher K_h, enhancing both effective diffusion (Eq. [6]) and the boundary layer mass transfer coefficient (Eq. [8]). Both effects influence period mean maximum flux density to a greater extent than cumulative flux, for which temperature effects tended to average out. Across scenarios, the maximum period mean flux sensitivity μ_{dEa} reflected the relative fraction of total volatilization associated with the tarped portion of the surface discussed above. In contrast, the 6-h mean flux density generally displayed low sensitivity to D_gE_a; this reflects the relatively weak temperature dependence of D_g (Table 1).

Sensitivity of Soil Gas Concentrations

Maximum shallow gas concentrations in the broadcast and bed scenarios displayed generally similar μ_i. In these scenarios, gas concentrations were relatively insensitive to variables solely related to volatile mass transfer across the tarped boundary layer (i.e., d and dE_a) but were sensitive to those involved in partitioning (K_h, K_hE_a, K_d, and ρ_b) and diffusion (θ_i, θ_s, and D_g). In all cases, k_1 had a negative effect on maximum shallow gas concentrations.

Soil gas concentrations were generally insensitive to ΔT, largely due to the offsetting effect of temperature-dependent factors that decrease the gas-phase concentration (k_1 and d) and increase fumigant gas concentrations (K_h). Temperature was important, however, in determining the 6-h period in which maximum gas concentrations were observed. In the bed scenario, 99% of maximum gas concentrations occurred in the 0600 to 1200 and 1200 to 1800 h time periods when surface soil temperatures were highest, while 66% of the maximum gas concentrations were similarly observed during the two high-temperature periods in the broadcast scenario. While temperature fluctuations at the 45-cm depth were only about 10% of those at the surface (Fig. 4c), maximum gas concentrations at that depth in the drip scenario also occurred at the higher temperature periods. Seventy-seven percent of maximum gas concentrations occurred during the 1800 to 2400 h time period in that scenario. This was the time of higher soil temperatures at that depth due to the phase lag between surface and subsurface soil temperatures (Fig. 4c).

For the drip application, the dominant mechanism for fumigant transport to the 45-cm depth under the line source was convection in moving water as opposed to diffusion in the gas phase. This was evident from simulation results (not shown) where D_g was set to zero. In those simulations, the median of simulated maximum gas concentrations 45 cm below the drip emitter was only 12% less than in corresponding simulations using identical input variables except with nonzero D_g. The role of convective transport in the drip scenario was also shown by the relatively high $\mu_{\lambda w}$, indicating the contribution of convective–dispersive transport as opposed to gaseous diffusion. In contrast to the broadcast and bed scenarios, maximum gas concentrations had a negative sensitivity to θ_s. This was attributable to a greater volume of water, hence fumigant, moving deep into the profile at low θ_s (Fig. 5).

Sensitivity Nonlinearity or Interactions

In several cases, the σ_i were large relative to their corresponding μ_i (Table 3), reflecting nonlinear effects of variables on model output or interactions between variables. An example of nonlinearity was the sensitivity of the maximum 6-h mean flux density to θ_i in the bed scenario. The individual $S_{\theta i}$ were significantly correlated with θ_i (Spearman $r = -0.74$, $P < 0.001$). Because $S_{\theta i}$ is essentially the derivative of the model output M with respect to θ_i, it is evident that changes in θ_i lead to much greater changes in the maximum 6-h mean flux density at higher values of θ_i (Fig. 6). In contrast, S_{Kh} values for maximum 6-h flux density in the drip scenario were only weakly dependent on K_h (Spearman $r = -0.31$, $P = 0.052$) but showed a strong interaction with d (Fig. 7).

Two general trends in nonlinearity or interaction were evident. First, there were significant interactions between θ_i and θ_s in the bed and broadcast scenarios, where volatilization was substantially mediated by the rate of diffusive transport. The interactive effect of these variables on flux was evident from significant Spearman correlations between $S_{\theta i}$ and θ_s, ranging from 0.39 to 0.53. Similarly, the correlations between $S_{\theta s}$ and θ_i ranged from 0.41 to 0.46. The interaction is attributable to their joint influence on D_{eff} (Eq. [6]). A second general result was that, while model outputs in all scenarios displayed a negative sensitivity to the fumigant degradation rate constant k_1, the effects were nonlinear. In all scenarios, the S_{k1} values of all model outputs were significantly correlated to the k_1 values themselves. Spearman correlations between S_{k1} and

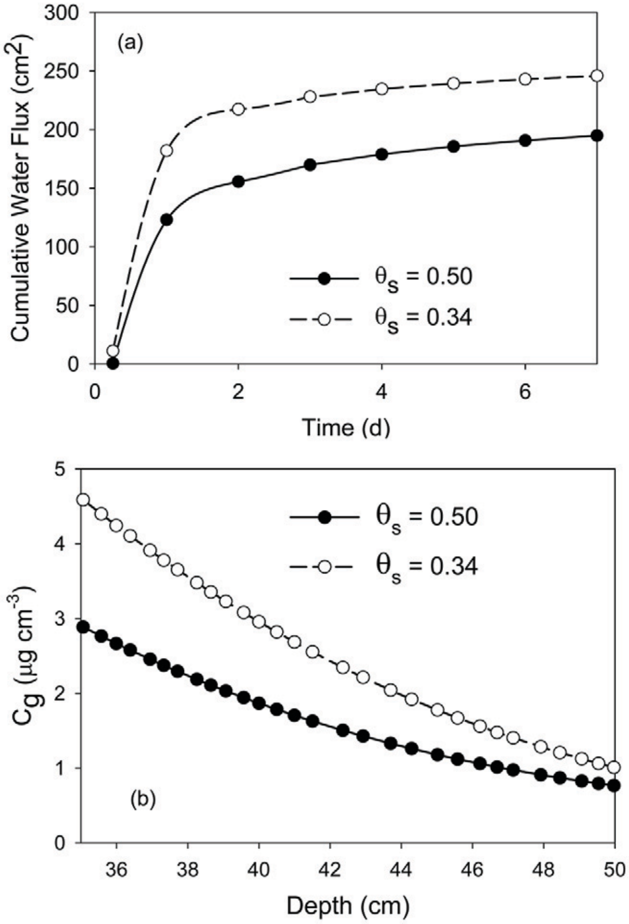

Fig. 5. Comparison of (a) cumulative water flux past the mesh line below dripper (mesh line location shown in Fig. 2), and (b) soil gas concentrations C_g across the depth range of 35 to 50 cm below the dripper for saturated water contents θ_s of 0.34 and 0.50.

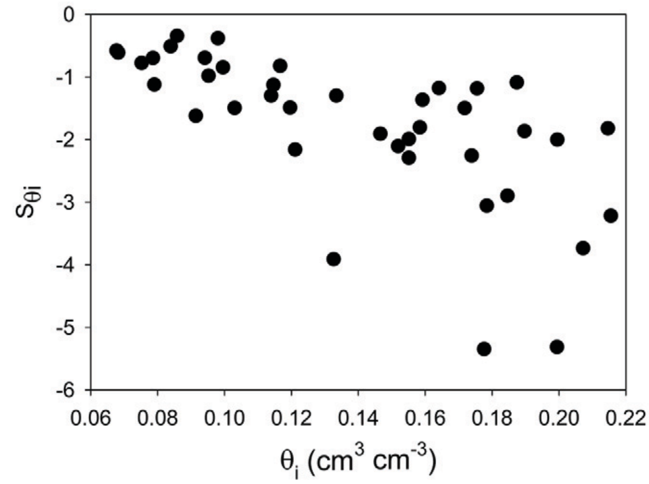

Fig. 6. Individual sensitivities of maximum 6-h mean flux densities (S) to initial water content θ_i, showing nonlinear effect of θ_i on maximum flux in the bed scenario.

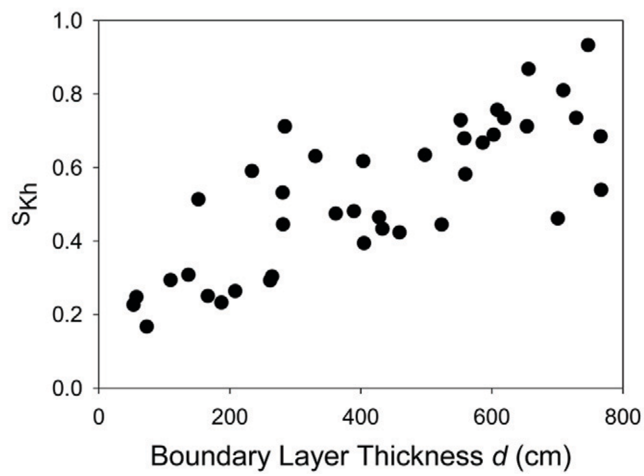

Fig. 7. Individual sensitivities of maximum 6-h mean flux densities to air–water partition coefficient K_h (S_{Kh}) vs. equivalent boundary layer depth d, showing interaction of K_h with d in the drip scenario.

k_1 ranged from −0.36 to −0.87, indicating a greater negative effect on model outputs for shorter degradation half-lives (higher k_1).

Discussion

The μ_i are estimates of the mean normalized partial derivative of model output with respect to each input. While they provide a general indication of variable influence on model output, knowledge of a variable's uncertainty or variability is also required for a relative assessment of contributions to model output uncertainty. For example, although flux predictions were very sensitive to D_g in some scenarios (Table 3), relatively accurate D_g estimation methods are available (e.g., Hilal et al., 2003a, 2003b; Tucker and Nelken, 1990). Consequently, the overall contribution of D_g to the uncertainty of modeled flux estimates is probably low. Similarly, accurate solubility and vapor pressure measurements should provide relatively accurate K_h estimates, particularly at the milligram per liter aqueous concentration ranges expected in the field (Smith and Harvey, 2007).

Most outputs were very sensitive to θ_s. A common modeling practice is to estimate θ_s based on soil texture class (Cryer and van Wesenbeeck, 2009; Luo et al., 2012; Yates et al., 2012). Schaap et al. (1998) reported a mean sandy loam θ_s of 0.389 with a standard deviation of 0.094 (N = 337 soils), greater than the 10% perturbation in θ_s used to estimate sensitivities here. Consequently, uncertainty in θ_s may contribute substantially to model output uncertainty. In addition to soil-to-soil variations within a texture class, management practices such as cultivation may result in temporal variations in θ_s within the same soil. Deviations between model predictions obtained using θ_s estimates may be potentially responsible for large differences between modeled and field-estimated fluxes. Alternatively, agreement between model and field-based fluxes may be observed when the model is actually not properly simulating field processes correctly—essentially providing the correct answer for the wrong reasons. In field studies where results are to be used as the basis for modeling, accurate site-specific determination of soil hydraulic properties is strongly preferred.

Model outputs were only moderately sensitive to the equivalent boundary layer d that describes tarp resistance to mass transfer. Tarp mass-transfer coefficients are sometimes highly variable, however, even among similar tarp–chemical combinations. Based on an estimated diffusion coefficient in air of 8899 $cm^2\ d^{-1}$, we calculated an iodomethane mean d of 1650 cm with a standard deviation of 1450 cm for 22 samples of unused virtually impermeable film (VIF) tarp based on the diffusive resistance data of Papiernik et al. (2011). In addition, the concordance of laboratory-measured permeabilities and actual field permeabilities are poorly understood, particularly given the potential for stretching and tears during application and the potentially high variation of VIF tarp permeability with humidity (Papiernik et al., 2011). Thus, for applications where a large fraction of fumigant volatilization may occur from tarped surfaces (e.g., broadcast or drip), accurate characterization of tarp-specific permeabilities is important. Otherwise uncertainty in d may substantially contribute to uncertainty in model predictions, limiting comparison with field-based flux estimates.

Model outputs were sensitive to degradation rates in all scenarios. Even when measured under well-controlled laboratory conditions, fumigant degradation rates vary substantially with soil type, moisture content, and temperature (Dungan and Yates, 2003). Fumigant degradation is similar to tarp permeability in the sense that the relationship between laboratory and field conditions is poorly understood. Consequently, degradation is potentially a major contributor to simulated estimates of flux in all scenarios.

The output variable sensitivities to the various activation energies that describe temperature dependence were generally low to moderate. For D_gE_a and K_hE_a, estimation methods applicable to environmental temperature ranges based on accepted physical chemistry theory are available (Smith and Harvey, 2007; Hilal et al., 2003a, 2003b; Tucker and Nelken, 1990). Obtaining reliable estimates for k_1E_a and dE_a is more difficult. Data for the temperature dependence of lumped degradation coefficients are sparse, although calculations for the limited fumigant aerobic degradation data that are available suggests a relatively narrow range of 40,000 to 65,000 J mol^{-1} for k_1E_a may be reasonable (Dungan and Yates, 2003; Gan et al., 2000; Guo and Gao, 2009). In the case of dE_a, the sensitivity of the broadcast maximum 6-h mean flux density was moderate. Data for dE_a are also sparse. Papiernik et al. (2011) measured the temperature dependence of the diffusion resistance across two VIF tarps for several fumigants. Their results showed differences of up to a factor of two. Actual dE_a measurements on the specific tarp–fumigant combination are recommended for site-specific simulations. This is particularly true in cases where a large fraction of volatilization occurs through the tarp (broadcast and drip scenarios) and when period mean flux densities are of primary interest.

Additional factors beyond the 15 variables evaluated here also influence flux and gas concentrations. These include chemical or organic soil amendments (McDonald et al., 2008), water applications (Gao et al., 2008; Gao and Trout, 2007), and the depth of fumigant application (Papiernik et al., 2004). Analysis of these factors was beyond the scope of this study. The sensitivity analysis provides insight into the relative importance of different transport mechanisms under different conditions, however, and will be useful in determining how such mitigation factors can be most efficiently implemented to reduce off-site fumigant air concentrations.

Conclusion

Different application scenarios yielded distinctly different sensitivity results. Interpreting the sensitivities from a mechanistic standpoint, we concluded that the μ_i are fundamentally related to the dominant transport and volatilization mechanisms in each scenario (i.e., Eq. [6] and [8]). Volatilization in the tarped broadcast scenario was mediated by diffusive transport and tarp mass transfer resistances in series. In that scenario, the cumulative flux sensitivity to boundary layer thickness was greatest, and the maximum 6-h mean fluxes were most sensitive to the boundary layer activation energy. In contrast, the bedded tarp fluxes were less sensitive to tarp parameters; volatilization occurred primarily through the untarped furrow regions. The effect of tarping was intermediate in the drip application, where the magnitude and relative contribution of volatilization through the tarped and untarped surfaces was dependent on both the rates of diffusive transport and soil hydraulic characteristics that influenced post-application fumigant and water penetration into the profile.

Based on this sensitivity analysis, uncertainty in three areas has the greatest potential to contribute to model uncertainty. These are (i) the fumigant degradation rate, (ii) soil water properties—both initial water content and saturated water content (i.e., porosity), and (iii) tarp permeability and permeability temperature dependence. The latter are primarily important in scenarios such as broadcast or near-surface drip application, where most or all volatilization occurs from a tarped soil surface.

References

Carsel, R.F., and R.S. Parrish. 1988. Developing joint probability distributions of soil water retention characteristics. Water Resour. Res. 24:755–769. doi:10.1029/WR024i005p00755

Chickos, J.S., and W.E. Acree, Jr. 2003. Enthalpies of vaporization of organic and organometallic compounds, 1880–2002. J. Phys. Chem. Ref. Data 32:519–878. doi:10.1063/1.1529214

Chung, S.O., and R. Horton. 1987. Soil heat and water flow with a partial surface mulch. Water Resour. Res. 23:2175–2186. doi:10.1029/WR023i012p02175

Crout, N., T. Kokkonen, A.J. Jakeman, J.P. Norton, L.T.H. Newham, R. Anderson, et al. 2008. Good modelling practice. In: A.J. Jakeman et al., editors, Environmental modelling, software and decision support: State of the art and new perspectives. Elsevier, Amsterdam.

Cryer, S.A., and I.J. van Wesenbeeck. 2009. Estimating field volatility of soil fumigants using CHAIN_2D: Mitigation methods and comparison against chloropicrin and 1,3-dichloropropene field observations. Environ. Monit. Assess. 15:309–318.

Cryer, S.A., and I.J. van Wesenbeeck. 2010. Coupling field observations, soil modeling, and air dispersion algorithms to estimate 1,3-dichloropropene and chloropicrin flux and exposure. J. Environ. Qual. 40:1450–1461. doi:10.2134/jeq2010.0130

Dungan, R.S., and R.S. Yates. 2003. Degradation of fumigant pesticides: 1,3-dichloropropene, methyl isothiocyanate, chloropicrin, and methyl bromide. Vadose Zone J. 2:279–286. doi:10.2136/vzj2003.2790

Gan, J., S.R. Yates, F.F. Ernst, and W.A. Jury. 2000. Degradation and volatilization of the fumigant chloropicrin after soil treatment. J. Environ. Qual. 29:1391–1397. doi:10.2134/jeq2000.00472425002900050004x

Gao, S., and T.J. Trout. 2007. Surface seals reduce 1,3-dichloropropene and chloropicrin emissions in field tests. J. Environ. Qual. 36:110–119. doi:10.2134/jeq2006.0107

Gao, S., T.J. Trout, and S. Schneider. 2008. Evaluation of fumigation and surface seal methods on fumigant emissions in an orchard replant field. J. Environ. Qual. 37:369–377. doi:10.2134/jeq2007.0088

Glew, D.N., and E.A. Moelwyn-Hughes. 1953. Chemical statics of the methyl halides in water. Discuss. Faraday Soc. 15:150–161. doi:10.1039/df9531500150

Guo, M., and S. Gao. 2009. Degradation of methyl iodide in soil: Effects of environmental factors. J. Environ. Qual. 38:513–519. doi:10.2134/jeq2008.0124

Ha, W., C.D. Stanley, R.S. Mansell, and H.A. Ajwa. 2009. 2-D Simulation of nonisothermal fate and transport of a drip-applied fumigant in plastic-mulched soil beds: II. Sensitivity analysis and model application. Transp. Porous Media 76:431–448. doi:10.1007/s11242-008-9256-2

Hilal, S.H., S.W. Karickhoff, and L.A. Carreira. 2003a. Prediction of chemical reactivity parameters and physical properties of organic compounds from molecular structure using SPARC. EPA/600/R-03/030. USEPA Natl. Expos. Res. Lab., Research Triangle Park, NC.

Hilal, S.H., S.W. Karickhoff, and L.A. Carreira. 2003b. Verification and validation of the SPARC model. EPA/600/R-03/033. USEPA Natl. Expos. Res. Lab., Research Triangle Park, NC.

Johnson, B., and F. Spurlock. 2009. Dominant soil types associated with fumigant applications in ozone nonattainment areas. Technical memorandum. Dep. Pest. Reg., Sacramento, CA. http://www.cdpr.ca.gov/docs/emon/pubs/ehapreps/eh4342.pdf.

Jury, W.A., W.F. Spencer, and W.J. Farmer. 1983. Behavior assessment model for trace organics in soil: I. Model description. J. Environ. Qual. 12:558–564. doi:10.2134/jeq1983.00472425001200040025x

Kim, J., S.K. Papiernik, W.J. Farmer, J. Gan, and S.R. Yates. 2003. Effect of formulation on the behavior of 1,3-dichloropropene in soil. J. Environ. Qual. 32:2223–2229. doi:10.2134/jeq2003.2223

Leij, F.J., W.J. Alves, M.Th. van Genuchten, and J.R. Williams. 1996. The UNSODA unsaturated soil hydraulic database: User's manual version 1.0. EPA/600/R-96/095. USEPA Natl. Risk Manage. Res. Lab., Cincinnati, OH.

Luo, L., D.A. Ashworth, J. Šimůnek, R. Xuan, and S.R. Yates. 2012. Assessment of methods for methyl iodide emission reduction and pest control using a simulation model. Atmos. Environ. 66:33–40. doi:10.1016/j.atmosenv.2012.03.080

Luo, L., S.R. Yates, and D.J. Ashworth. 2011. Predicting methyl iodide emission, soil concentration, and pest control in a two-dimensional chamber system. J. Environ. Qual. 40:109–117. doi:10.2134/jeq2010.0280

Majewski, M.S. 1997. Error evaluation of methyl bromide aerodynamic flux measurements. ACS Symp. Ser. 652:135–153.

Marty, M., F. Spurlock, and T. Barry. 2010. Volatile organic compounds from pesticide application and contribution to tropospheric ozone. In: R. Krieger, editor, Hayes' handbook of pesticide toxicology. 3rd ed. Academic Press, London. p. 571–586.

McDonald, J.A., S. Gao, R. Qin, T.J. Trout, and B.D. Hanson. 2008. The effect of chemical and manure amendment with water application and tarp on 1,3-dichloropropene emissions from soil. Environ. Sci. Technol. 42:398–402. doi:10.1021/es071133o

McKay, M.D., R.J. Bechman, and W.J. Conover. 1979. A comparison of three methods for selecting values of input variables in the analysis of output from a computer code. Technometrics 21:239–245.

Moldrup, P., T. Olesen, J. Gamst, P. Schjonning, T. Yamaguchi, and D.E. Rolston. 2000. Predicting the gas diffusion coefficient in repacked soil: Water-induced linear reduction model. Soil Sci. Soc. Am. J. 64:1588–1594. doi:10.2136/sssaj2000.6451588x

Morris, M.D. 1991. Factorial sampling plans for preliminary computational experiments. Technometrics 33:161–174. doi:10.1080/00401706.1991.10484804

Papiernik, S.K., R.S. Dungan, W. Zheng, M. Guo, S.M. Lesch, and S.R. Yates. 2004. Effect of application variables on emissions and distribution of fumigants applied via subsurface drip irrigation. Environ. Sci. Technol. 38:5489–5496. doi:10.1021/es049064q

Papiernik, S.K., S.R. Yates, and D.O. Chellimi. 2011. A standardized approach for estimating the permeability of plastic films to soil fumigants under various field and environmental conditions. J. Environ. Qual. 40:1375–1382. doi:10.2134/jeq2010.0118

Petersen, L.W., P. Moldrup, O.H. Jacobsen, and D.E. Rolston. 1996. Relations between specific surface area and soil physical and chemical properties. Soil Sci. 161:9–21. doi:10.1097/00010694-199601000-00003

Radcliffe, D.E., and J. Šimůnek. 2010. Soil physics with HYDRUS: Modeling and applications. CRC Press, Boca Raton, FL.

Ross, L.J., B. Johnson, K.D. Kim, and J. Hsu. 1996. Prediction of methyl bromide flux from area sources using the ISCST model. J. Environ. Qual. 25:885–891. doi:10.2134/jeq1996.00472425002500040033x

Ruzo, L.O. 2006. Physical, chemical and environmental properties of selected chemical alternatives for the pre-plant use of methyl bromide as soil fumigant. Pest Manage. Sci. 62:99–113. doi:10.1002/ps.1135

Saltelli, A., M. Ratto, S. Tarantola, and F. Campolongo. 2005. Sensitivity analysis for chemical models. Chem. Rev. 105:2811–2828. doi:10.1021/cr040659d

Schaap, M.G., F.J. Leij, and M.Th. van Genuchten. 2001. ROSETTA: A computer program for estimating soil hydraulic parameters with hierarchical pedotransfer functions. J. Hydrol. 251:163–176. doi:10.1016/S0022-1694(01)00466-8

Schaap, M.G., F.J. Leij, and M.Th. van Genuchten. 1998. Neural network analysis for hierarchical prediction of soil hydraulic properties. Soil Sci. Soc. Am. J. 62:847–855. doi:10.2136/sssaj1998.03615995006200040001x

Šimůnek, J., M. Šejna, H. Saito, M. Sakai, and M.Th. van Genuchten. 2008a. The HYDRUS-1D software package for simulating the one-dimensional movement of water, heat, and multiple solutes in variably-saturated media. Version 4.0. HYDRUS Softw. Ser. 3. Dep. of Environ. Sci., Univ. of California, Riverside.

Šimůnek, J., and M.Th. van Genuchten. 1994. The CHAIN-2D code for simulating two-dimensional movement of water flow, heat, and multiple solutes in variably-saturated porous media. Version 1.1. Res. Rep. 136. U.S. Salinity Lab., Riverside, CA.

Šimůnek, J., M.Th. van Genuchten, and M. Šejna. 2008b. Development and applications of the HYDRUS and STANMOD software packages, and related codes. Vadose Zone J. 7:587–600. doi:10.2136/VZJ2007.0077

Šimůnek, J., M.Th. van Genuchten, and M. Šejna. 2011. The HYDRUS software package for simulating two- and three dimensional movement of water, heat, and multiple solutes in variably-saturated media. Version 2.0. PC-Progress, Prague, Czech Republic.

Smith, F.L., and A.H. Harvey. 2007. Avoid common pitfalls when using Henry's Law. Chem. Eng. Prog. 103:33–39.

Sullivan, D.A., M.T. Holdsworth, and D.J. Hlinka. 2004. Monte Carlo-based dispersion modeling of off-gas releases from the fumigant meta-sodium for determining distances to exposure endpoints. Atmos. Environ. 38:2471–2481. doi:10.1016/j.atmosenv.2004.02.001

Tucker, W.A., and L.H. Nelken. 1990. Diffusion coefficients in air and water. In: W.J. Lyman et al., editors, Handbook of chemical property estimation methods. Am. Chem. Soc., Washington, DC. p. 17-1–17-24.

USEPA. 2001. Correcting the Henry's Law constant for soil temperature. Fact Sheet. USEPA Ecosyst. Res., Athens, GA. http://www.epa.gov/athens/learn2model/part-two/onsite/doc/factsheet.pdf.

van den Berg, F., D.J. Brus, S.L.G.E. Burgers, G.B.M. Heuvelink, J.G. Kroes, J. Stolte, et al. 2008. Uncertainty and sensitivity analysis of GeoPEARL. Alterra Rep. 1330. PBL Rep. 500123001. Alterra, Wageningen, the Netherlands. http://www.pearl.pesticidemodels.nl/pdf/report_1330.pdf

van Genuchten, M.Th. 1980. A closed-form equation for predicting the hydraulic conductivity of unsaturated soils. Soil Sci. Soc. Am. J. 44:892–898. doi:10.2136/sssaj1980.03615995004400050002x

van Griensven, A., T. Meixner, S. Grunwald, T. Bishop, M. Diluzio, and R. Srinivasan. 2006. A global sensitivity analysis tool for the parameters of multi-variable catchment models. J. Hydrol. 324:10–23. doi:10.1016/j.jhydrol.2005.09.008

Wang, L., D.B. Parker, C.B. Parnell, R.E. Lacey, and B.W. Shaw. 2006. Comparison of CALPUFF and ISCST3 models for predicting downwind odor and source emission rates. Atmos. Environ. 40:4663–4669. doi:10.1016/j.atmosenv.2006.04.043

Warren-Hicks, W., J.P. Carbone, and P.L. Havens. 2002. Using Monte Carlo analysis to judge model prediction accuracy: Validation of the Pesticide Root Zone Model 3.12. Environ. Toxicol. Chem. 21:1570–1577. doi:10.1002/etc.5620210807

Yates, S.R. 2009. Analytical solution describing pesticide volatilization from soil affected by a change in surface condition. J. Environ. Qual. 38:259–267. doi:10.2134/jeq2008.0059

Yates, S.R., D. Ashworth, and L. Luo. 2012. Reducing emissions of volatile organic compounds (VOCs) from agricultural soil fumigation: Comparing emission estimates using simplified methodology. U.S Salinity Lab., Riverside, CA. www.arb.ca.gov/research/rsc/10-28-11/item4dfr07-332.pdf

Yates, S.R., D. Wang, S.K. Papiernik, and J. Gan. 2002. Predicting pesticide volatilization from soils. Environmetrics 13:569–578. doi:10.1002/env.542